Medical Image Analysis 56 (2019) 184–192

Contents lists available at ScienceDirect

Medical Image Analysis

journal homepage: www.elsevier.com/locate/media

A methodology for generating four-dimensional arterial spin labeling MR angiography virtual phantoms

Renzo Phellan[a,*], Thomas Lindner[b], Michael Helle[c], Alexandre X. Falcão[d], Thomas W. Okell[e], Nils D. Forkert[a]

[a] Department of Radiology and Hotchkiss Brains Institute University of Calgary, Calgary, AB, Canada
[b] Clinic for Radiology and Neuroradiology University Medical Center Schleswig-Holstein, Kiel, Germany
[c] Philips Technologie GmbH Innovative Technologies, Hamburg, Germany
[d] Laboratory of Image Data Science Institute of Computing University of Campinas, Campinas, SP, Brazil
[e] Wellcome Centre for Integrative Neuroimaging FMRIB Nuffield Department of Clinical Neurosciences University of Oxford, Oxford, United Kingdom

ARTICLE INFO

Article history:
Received 14 November 2018
Revised 31 May 2019
Accepted 11 June 2019
Available online 13 June 2019

Keywords:
Angiography
Cerebrovascular imaging
Arterial spin labeling
Blood flow analysis
Phantom models

ABSTRACT

Four-dimensional arterial spin labeling magnetic resonance angiography (4D ASL MRA) is a non-invasive medical imaging modality that can be used for anatomical and hemodynamic analysis of the cerebrovascular system. However, it generates a considerable amount of data, which is tedious to analyze visually. As an alternative, medical image processing methods can be used to process the data and present measurements of the geometry and blood flow in the cerebrovascular system to the user, such as vessel radius, tortuosity, blood flow volume, and transit time. Nevertheless, evaluating medical image processing methods developed for this modality requires annotated data, which can be time-consuming and expensive to obtain. Alternatively, virtual simulations are a faster and less expensive option that can be used for initial evaluation of image processing methods. The present work proposes a methodology for generating annotated 4D ASL MRA virtual phantoms, in different scenarios with different acquisition parameter settings. In each scenario, the phantoms are generated using real cerebrovascular geometries of healthy volunteers, where blood flow is simulated according to a mathematical model specifically designed to describe the signal observed in 4D ASL MRA images. Realistic noise is added using an homomorphic approach, designed to replicate noise characteristic of multi-coil acquisitions. In order to exemplify the utility of the phantoms, they are used to evaluate the accuracy of a method to estimate blood flow parameter values, such as relative blood volume and transit time, in different scenarios. The estimated values are then compared to its corresponding virtual ground-truth values. The accuracy of the results is ranked according to the average absolute error. The results of the experiments show that blood flow parameters can be more accurately estimated when blood is magnetically labeled for longer periods of time and when the datasets are acquired with higher temporal resolution. In summary, the present work describes a methodology to create annotated virtual phantoms, which represent a useful alternative for initial evaluation of medical image processing methods for 4D ASL MRA images.

1. Introduction

Cerebrovascular diseases are among the top ten causes of death according to the global report published by the World Health Organization, with increasing prevalence over the last fifteen years (Department of information, evidence and research of the World Health Organization, 2017). Four-dimensional arterial spin labeling magnetic resonance angiography (4D ASL MRA) is a non-invasive medical imaging modality that can be used for investigation of the anatomical structure and blood flow of the cerebrovascular system at high spatial and temporal resolution (Robson et al., 2010). Therefore, this rather new MRA imaging technique has high potential to support diagnosis, treatment planning, and follow-up assessment of cerebrovascular diseases, such as aneurysms, arteriovenous-malformations, stenosis, and stroke. However, 4D ASL MRA generates a considerable amount of data, which is time-consuming and tedious to analyze directly. A solution to this problem is using medical image processing methods to process the data, in order to extract the information contained in 4D ASL MRA images (Phellan et al., 2018b). This information includes geometric measurements of the vascular system, such as

* Corresponding author.
E-mail address: phellan.renzo@ucalgary.ca (R. Phellan).

https://doi.org/10.1016/j.media.2019.06.002
1361-8415/

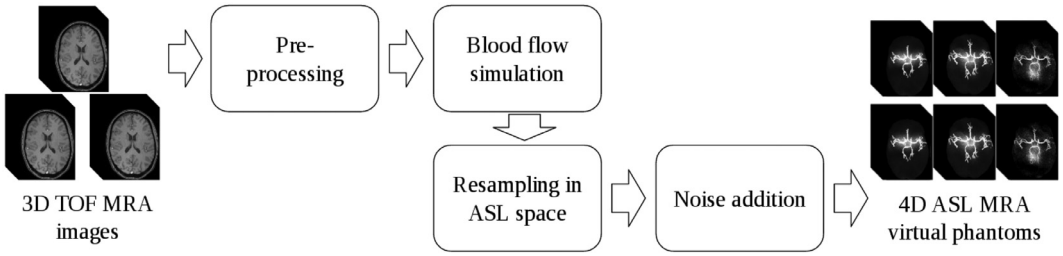

Fig. 1. Diagram of the proposed methodology for 4D ASL MRA virtual phantoms generation.

vessel radius, tortuosity, and density, and hemodynamic measurements, e.g. blood flow volume and transit time.

Developing and evaluating the novel image processing methods for 4D ASL MRA usually requires annotated datasets, with geometric and blood flow ground-truth values. These datasets are time-consuming and expensive to obtain (Hamarneh and Jassi, 2010). Alternatively, virtual phantoms are a faster and less expensive option for initial evaluation of medical image processing methods. Some examples include the BrainWeb database (Cocosco et al., 1997), which contains simulated brain magnetic resonance images with configurable parameter settings. Additionally, the software VascuSynth Hamarneh and Jassi (2010) allows the creation of volumetric images of a vascular tree with corresponding ground-truth geometries, but no blood flow data. Finally, a simulation of blood flow in the cerebral venous system was proposed as part of the VIVABRAIN project (Miraucourt et al., 2017). In this case, subject-specific geometries are used as the basis for blood flow simulation employing the Navier-Stokes equations for incompressible viscous fluid. Currently, to the best of our knowledge, no virtual phantoms are available to evaluate medical image processing methods specifically for 4D ASL MRA series.

The first objective of the present study is to present a methodology to create annotated virtual phantoms of 4D ASL MRA series from subject-specific geometries, based on a mathematical model of the blood flow specifically designed to describe the temporal signal measured by this imaging modality (Okell et al., 2010). Additionally, in order to achieve a realistic simulation, noise is added using an homomorphic approach (Aja-Fernández et al., 2015), designed to replicate noise characteristic of multi-coil acquisitions. The second objective is to compare the accuracy of a blood flow parameter estimation method using phantoms generated with different acquisition parameters. The source code developed as part of this project to generate the phantoms is available online (Phellan, 2019).

2. Materials and methods

2.1. Materials

Local institutional ethics committee (Ärztekammer Schleswig-Holstein and Calgary Health Regional Ethic Board) approval was obtained and all subjects provided written informed consent consistent with the Declaration of Helsinki prior to study participation.

3D multi-slab time-of-flight (TOF) MRA images were acquired from ten volunteers using a Philips Achieva 3T MRI scanner (Philips Healthcare, Best, The Netherlands), with a standard 32-channel head coil. Only healthy subjects without any history of cerebrovascular or neurological diseases were included. Each TOF MRA image is composed of 171 slices with 512 × 512 voxels, with voxel size 0.41 × 0.41 × 0.70 mm^3. A flow compensated readout was used, with SENSE factor 2, TR = 20 ms, TE = 3.45 ms, flip angle 20°, and half scan factor 0.7. The total scan time was 6:39 min. TOF MRA images can capture the subjectsâ cerebrovascular geometry with higher spatial resolution than 4D ASL MRA, but they do not contain any temporal data.

Additionally, corresponding 4D ASL MRA series were acquired from the same volunteers using the same scanner during the same imaging session, for qualitative comparison of the proposed virtual phantom datasets. Each 4D ASL MRA series contains six three-dimensional control/labeled image pairs that display the passage of magnetically labeled blood through the cerebrovascular system, with a temporal resolution of 120*ms*. Each image contains 120 slices of 224 × 224 voxels, with voxel size 0.94 × 0.94 × 1.0 mm^3, from the base of the neck to the top of the head. Image acquisition was performed using pseudo-continuous ASL and a Look-Locker readout to speed up the process. A T1-Turbo Field Echo (TFE) scan was employed, with TFE factor 16, SENSE factor 3, TR = 7.7 ms, TE = 3.7 ms, flip angle 10°, and half scan factor 0.7. The blood was magnetically labeled for 300 ms. The SENSE factor was only applied in the phase-encoding direction because extensive pulsation artifacts were noted in case of application in the through-slice directions. The total scan time was 5 min.

Fig. 1 shows the proposed methodology to create 4D ASL MRA virtual phantoms, described in more detail in the following. Because of the higher spatial resolution of TOF MRA images compared to 4D ASL MRA series, blood flow parameter values are initially simulated in TOF MRA space and then resampled to 4D ASL space taking partial volume effects into account. The real 4D ASL MRA images acquired for this work are only used as a reference, and they are not required to create the phantoms.

2.2. Pre-processing

As this work focuses on arteries in the brain, all ten TOF MRA images acquired from healthy volunteers are skull-stripped using a fully automatic segmentation algorithm (Forkert et al., 2009). Then, the cerebrovascular system is segmented in the TOF MRA images using a validated automatic method (Forkert et al., 2013), generating ten binary segmentations. For creation of the 4D ASL MRA virtual phantoms, the ten TOF MRA binary vessel segmentations are divided into three main vascular territories, depending on the main feeding artery: left internal carotid artery (LICA), right internal carotid artery (RICA), or basilar artery (BA). For simplicity reasons, it is assumed that only one artery feeds each territory, so that there is no mixing of blood originating from different arteries. This is a reasonable assumption for healthy subjects (Okell et al., 2010), and it simplifies the computational calculations described below. The separation of the full arterial tree into the three main vessel territories is performed in this work using the image foresting transform algorithm (IFT) (Falcão et al., 2004). The IFT is a graph-based path optimization algorithm that requires the manual selection of three seed voxels at the origin of each main artery territory (LICA, RICA, and BA), which can be seen in Fig. 2A. Then, the IFT algorithm assigns each non-seed voxel in the binary segmentation to a feeding artery by identifying the most closely connected seed voxel (i.e., the one that is associated with the

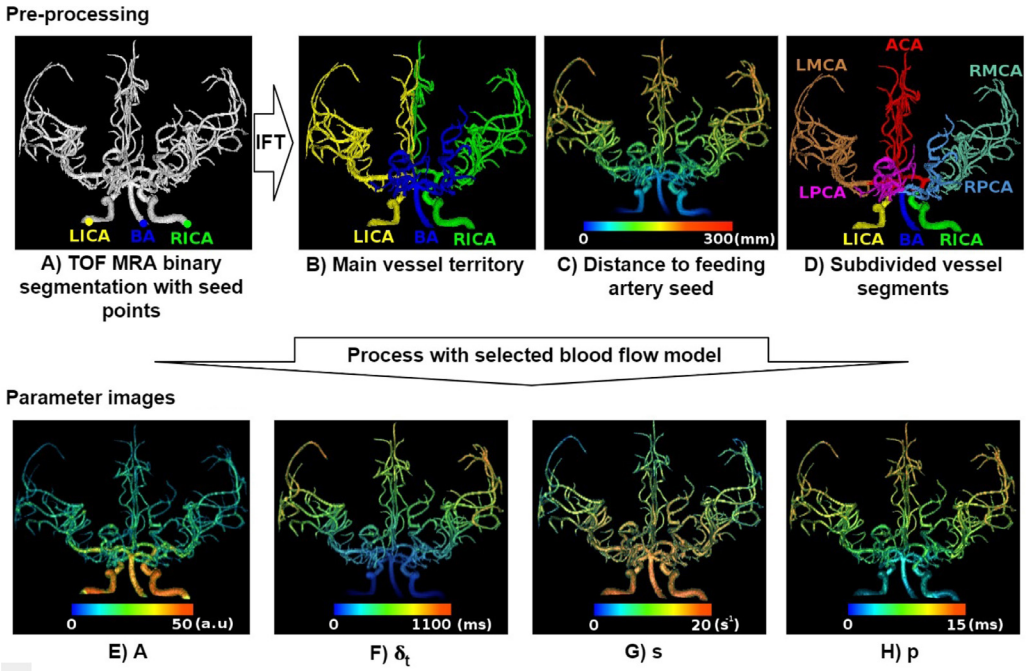

Fig. 2. 3D visualizations of the pre-processing steps and resulting blood flow parameter images. A is a scaling factor, proportional to the blood volume; δ_t is the blood transit time from the labeling plane to any artery; and s and p are the sharpness and time-to-peak of the distribution that models the dispersion of blood as it flows trough the cerebrovascular system.

minimum path length). Fig. 2 shows 3D visualizations of the resulting images after applying the IFT algorithm to identify the LICA, RICA, and BA vessel territories. As it can be noted, the IFT generates both, a main vessel territory map (Fig. 2B) and a map that displays the length of the path from each manually selected seed voxel in a main feeding artery to every other voxel that belongs to this artery (Fig. 2C).

The last pre-processing step aims at defining blood flow velocities for the extracted vessels. Since no velocity measurements such as phase-contrast MRA datasets were available, population-based normative values were used in this work instead. Therefore, the three main vessel territories (LICA, RICA, and BA) were further manually subdivided into the left and right posterior cerebral arteries (LPCA and RPCA), left and right middle cerebral arteries (LMCA and RMCA), and anterior cerebral artery (ACA) (Fig. 2D). After this step, population-based blood flow values were randomly selected within the ranges reported by Zarrinkoob et al. (2015), and assigned to the LICA, RICA, and BA sections. In order to conserve the mass of blood in the system, the flow is then distributed to the LPCA, RPCA, LMCA, RMCA, and ACA, according to the proportions described by Zarrinkoob et al. (2015), assuming no mixture of blood. Finally, the blood flow is distributed equally at every branching point within the previously listed artery sections. This is a reasonable assumption considering that no flow measurements have been reported at this level of detail, due to the considerable inter-subject variability of the small vessels in the cerebrovascular system.

Once the blood flow values are assigned to every segment of the cerebrovascular system, the blood flow velocities V are estimated according to the formula shown in Eq. (1), where F denotes blood flow, and A the cross sectional area of a vascular segment. The feasibility of the resulting velocities is automatically verified by comparison to corresponding reference values and ranges reported by MacDonald and Frayne (2015).

$$F = A \times V \tag{1}$$

2.3. Parameter and blood flow images

After identification of the vascular segments, the mathematical model proposed by Okell et al. (2010) specifically developed for 4D ASL MRA image series is used to simulate the time curve S representing the signal of magnetically labeled blood flowing through the cerebrovascular system for each voxel. This model is selected because it is one of the few in the scientific literature that describes the 4D ASL MRA measured signal of labeled blood as it flows through the brain arteries, before reaching the capillaries and perfusing the brain tissue. The model is presented in Eq. (2).

$$S(u,t) = \int_{t-\delta_t-\tau}^{t-\delta_t} A(u)\, dt_d\, D(u,t_d)\, T(\delta_t,t_d)\, R(t) \tag{2}$$

$$D(u,t_d) = \begin{cases} s(\Gamma(1+ps))^{-1} \exp(-st_d)(st_d)^{ps} & \text{if } st_d > 0,\ ps > -1 \\ 0 & \text{otherwise} \end{cases} \tag{3}$$

$$T(\delta_t,t_d) = \exp(-(\delta_t + t_d)/T_{1b}) \tag{4}$$

$$R(t) = \cos(\alpha)^{(t-t_0)/TR} \sin(\alpha) \tag{5}$$

Here, $S(u,t)$ is the signal in voxel u, at time t, τ is the magnetic blood labeling time, δ_t is the blood transit time from the labeling plane to the voxel u, and t_d is the additional time delay caused by dispersion of the blood before reaching the voxel u. The term $A(u)$ is a scaling factor, which is proportional to the blood volume. This last term includes a calibration factor S_0 in its formulation, which accounts for the equilibrium magnetization of blood M_{0b}.

The term $D(u,t_d)$ in Eq. (3) is a distribution that models the dispersion of labeled blood. It depends on the parameters s and p, which control the sharpness and time to peak of the distribution, respectively. The gamma function (Γ) is used to normalize the distribution. The term $T(\delta_t,t_d)$ in Eq. (4) models the signal attenuation

Table 1
Descriptions of the terms and parameters used for blood flow simulation.

Term	Description
u	Voxel being analyzed.
t	Time transcurred since the start of the acquisition process.
$S(u, t)$	Signal in voxel u, at time t.
τ	Time the blood is magnetically labeled.
δ_t	Blood transit time from the labeling plane to the voxel u.
t_d	Time delay caused by dispersion of the blood.
$A(u)$	Scaling factor, proportional to the blood volume in voxel u.
$D(u, t_d)$	Distribution that models the dispersion of labeled blood.
s	Sharpness of $D(u, t_d)$.
p	Time-to-peak of $D(u, t_d)$.
$\Gamma(x)$	Gamma function.
$T(\delta_t, t_d)$	Signal attenuation due to T_1 decay.
T_{1b}	Longitudinal relaxation time of arterial blood.
$R(t)$	Signal attenuation due to imaging radiofrequency pulses.
α	Flip angle.
t_0	Time at which the first imaging pulse is applied.
TR	Repetition time.

due to T_1 decay, where T_{1b} is the longitudinal relaxation time of arterial blood. The value of T_{1b} at 3T is estimated as 1664 $\pm$ 14 ms (Lu et al., 2004). Finally, the term $R(t)$ (Eq. (5)) accounts for the signal attenuation due to imaging radiofrequency pulses applied to the labeled blood as it reaches its destination. The parameter α corresponds to the flip angle associated to the imaging pulse, t_0 is the time at which the first imaging pulse is applied, and TR is the repetition time. The model assumes that all transverse magnetization is spoiled at the end of every TR, so that the longitudinal magnetization is reduced by a factor of $\cos(\alpha)$ with every pulse. In this work, the simplified version of the term $R(t)$, proposed by Okell et al. (2010), is used under the assumption that the imaging region comprises only anatomical structures distal to the labeling plane. Finally, the term $\sin(\alpha)$ accounts for the amount of transverse magnetization generated from a given amount of longitudinal magnetization. A summary of the terms and parameters used for blood flow simulation is presented in Table 1.

To calculate the temporal signal curve $S(u, t)$ for each voxel u at time t in a 4D ASL MRA series, the following parameters must be known or estimated: $A(u)$, δ_t, s, p, τ, T_{1b}, α, t_0, and TR. The first four are blood flow parameters, where the volume $A(u)$ is assumed to be proportional to the square of the artery radius, according to the Hagen-Poiseuilleâs law (Hagen, 1839; Poiseuille, 1844). The radius of each artery is obtained from the subject-specific artery geometries by using an image processing algorithm that calculates the distance of every voxel in the skeleton of an artery to the closest non-artery voxel. The skeleton values are then propagated within each voxel's region of influence, according to a Voronoi map (Phellan and Forkert, 2017). The largest artery in a binary segmentation is assigned the maximum relative volume value selected for the simulations, and the other arteries are assigned relative volume values proportional to the square of their radius over the square of the largest artery radius. The blood arrival time δ_t is calculated for each voxel by dividing the path length from the distance map by the average blood flow velocity along the path from the corresponding seed voxel. The parameters s and p vary inversely proportionally and proportionally to the path length indicated in the distance map, respectively (Okell et al., 2010). For automatic definition of s and p for every artery voxel, the artery voxels with path length value of 0 in the distance map are assigned predefined maximum s and minimum p values of 15 s^{-1} and 0 ms, respectively, and the artery voxels with maximum path length value are assigned predefined minimum s and maximum p values of 0 s^{-1} and 15 ms, respectively. For all other artery voxels, s and p values are interpolated by considering their corresponding path length. The minimum and maximum s and p values are obtained from the results of the experiments reported by Okell et al. (2010). Fig. 2 shows an example of the parameter values $A(u)$, δ_t, s, and p (Fig. 2E–H respectively) for a whole cerebrovascular system. The remaining five variables are image acquisition parameters (τ, T_{1b}, α, t_0, and TR), which are defined according to the different scenarios evaluated in this work described below.

The simulated 4D ASL MRA datasets and the corresponding blood flow parameter images, generated in TOF MRA space are resampled into the 4D ASL MRA space by using linear interpolation, which adds partial volume effects to the process. Fig. 3 shows a simulated 4D ASL MRA series. Additionally, to generate vascular ground-truth segmentations for the resampled 4D ASL MRA series, a temporal maximum intensity projection was calculated and thresholded at a low signal intensity value $th = 0.0001$. This leads to a precise segmentation as no noise artefacts are present in the simulated and downsampled images yet.

2.4. Noise addition

The real 4D ASL MRA datasets used as a reference to create the simulated datasets were acquired using a standard 32-channel head coil, with SENSE reconstruction. In this case, the noise present in the magnitude of the signal can be assumed to follow a Rician distribution (Aja-Fernández et al., 2014).Additionally, the variance of the noise (σ^2) is expected to vary locally in the image as a consequence of the multi-coil acquisition (Aja-Fernández et al., 2015).

A homomorphic approach (Aja-Fernández et al., 2015) was used in this work in order to replicate the Rician noise from real datasets in the simulated datasets. The main advantage of this approach is that it does not require additional information regarding the acquisition of the datasets to estimate the noise parameters, such as multiple acquisitions, biophysical models, or coil sensitivity estimations (Aja-Fernández et al., 2014).

Practically, the freely available implementation described by Kiepas and Sieradzki (2015)was applied in this work in a slice-by-slice manner to each control/labeled pair of images of a real dataset. The algorithm computes a map with the noise variance (σ^2) for each voxel of an image that belongs to a 4D ASL MRA dataset. After this, noise images are generated for each control and

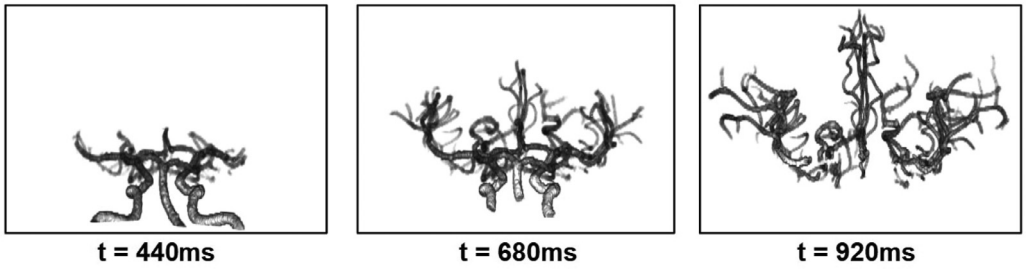

Fig. 3. 3D renderings of three images of the simulated 4D ASL MRA series, for t = 440, 680, and 920 ms (scenario 1).

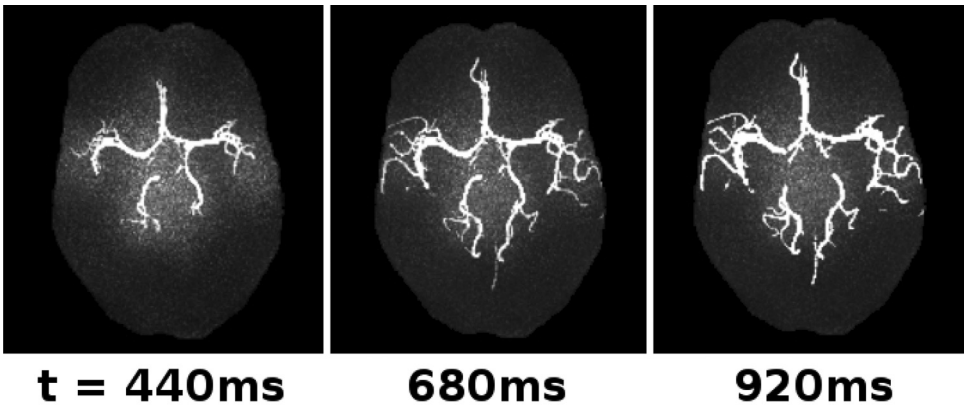

Fig. 4. Maximum intensity projections of 30 contiguous slices of three images of the simulated 4D ASL MRA series, for t = 440, 680, and 920 ms (scenario 1).

Table 2
Acquisition parameter values and times in each scenario, based on configuration described by Phellan et al. (2018b) (scenarios 1–4), Okell et al. (2010) (scenarios 5–8), and Kopeinigg and Bammer (2014) (scenarios 9–12).

Scen.	r (ms)	τ (ms)	α (°)	t_0 (ms)	TR (ms)	Interval (ms)	n
1	35	300	10	320	7.5	320–915	18
2	55	300	10	320	7.5	320–925	12
3	90	300	10	320	7.5	320–950	8
4	120	300	10	320	7.5	320–920	6
5	35	1000	20	1015	18	1015–2065	31
6	55	1000	20	1015	18	1015–2060	20
7	90	1000	20	1015	18	1015–2095	13
8	120	1000	20	1015	18	1015–2095	10
9	35	3000	6	3000	7.2	3000–5590	75
10	55	3000	6	3000	7.2	3000–5585	48
11	90	3000	6	3000	7.2	3000–5520	29
12	120	3000	6	3000	7.2	3000–5520	22

label image and simulated time point using the determined local noise variance for each voxel. The generated noise images of each control and label image pair are subtracted and the resulting noise image is added to the corresponding simulated 4D ASL image. Fig. 4 shows an example of a simulated 4D ASL MRA dataset, with added noise.

3. Experiments

In order to exemplify the utility of the virtual phantoms, they are used to evaluate the accuracy of a blood flow parameter estimation method. Given the degree of freedom of the 4D ASL MRA phantoms with respect to the acquisition parameters, twelve scenarios are generated, as described below, for which the blood flow parameter estimation method is evaluated.

3.1. Simulation scenarios

Twelve different 4D ASL MRA image series were generated for each of the ten subjects available using different acquisition parameter settings for the simulations. More precisely, the voxel-wise blood flow parameters $A(u)$, δ_t, s, and p were kept the same in all scenarios, but different values were used for the acquisition parameters τ, α, t_0, and TR (Table 2). The temporal resolution of the simulated series (r) is also reported, together with the different time intervals when images are acquired, and the number of images (n) within those intervals (see Table 2). T_{1b} has a constant value, as all images are simulated to be acquired at a magnetic field strength of 3T.

It is important to notice that the temporal resolution used in each scenario is restricted by the configuration of acquisition parameters used. All evaluated scenarios are feasible since configurations reported in the scientific literature were used for this (Kopeinigg and Bammer, 2014; Okell et al., 2010; Phellan et al., 2018b).

3.2. Blood flow parameter estimation method

A common method for blood flow parameter estimation is to fit a mathematical model containing the parameters to be estimated to the observed signal over time, for each voxel that belongs to an artery of interest in the brain. In this work, the same model used to generate the phantoms (Okell et al., 2010) is selected for curve fitting to the simulated 4D ASL MRA signal. It should be noted that the signal present in the 4D ASL MRA virtual phantoms has been affected by partial volume effects and Rician noise addition, so that using the same model for blood flow parameter estimation is not expected to lead to the original parameter values.

A typical approach to fit a hemodynamic model function to discrete concentration time curves for hemodynamic analysis is to use an optimization method, e.g. by minimizing the sum of squared differences between the measured curve and the optimized model using the Powell algorithm or other algorithms (Forkert et al., 2011). In this work, the blood flow parameter values are optimized using the Multi-Scale Parameter Search (MSPS) algorithm, which has been proven to be suitable for medical image processing tasks (Phellan et al., 2018b; Ruppert et al., 2017).

The MSPS algorithm requires a set of scales for each parameter for the optimization process. Larger scales allow the MSPS to avoid getting stuck in local minima, and smaller scales help to refine the final solution. In each iteration, the MSPS algorithm dislocates in the search space using all possible combinations of scales for all parameters, finds the optimal location, and moves to it. The process is repeated until the change observed in the function being optimized is below a set threshold. In this work, eight scales were found to be a reasonable compromise between processing time and the accuracy of the fit. The scales used in this work for each parameter are: $A(u) = \{0.01, 0.05, 0.1, 0.5, 1.0, 5.0, 10.0, 50.0\}$ *a.u.*, $\delta_t = \{0.001, 0.01, 0.1, 1.0, 5.0, 10.0, 50.0, 100.0\}$ ms, $s = \{0.01, 0.05, 0.1, 0.5, 1.0, 2.0, 5.0, 10.0\}$ s^{-1}, and $p = \{0.01, 0.05, 0.1, 0.5, 1.0, 2.0, 5.0, 10.0\}$ ms, which were defined considering the magnitude of the values observed in the results of the experiments reported by Okell et al. (2010). The MSPS search space was addittionally restricted in this work to avoid negative values for any parameter.

The MSPS search process minimizes the average absolute error (AAE) between the precalculated temporal signal curve using a set of blood flow parameters, and the discrete sample points for each voxel of the 4D ASL dataset. The AAE is preferred as a metric over the average sum of squared errors because fitting errors with

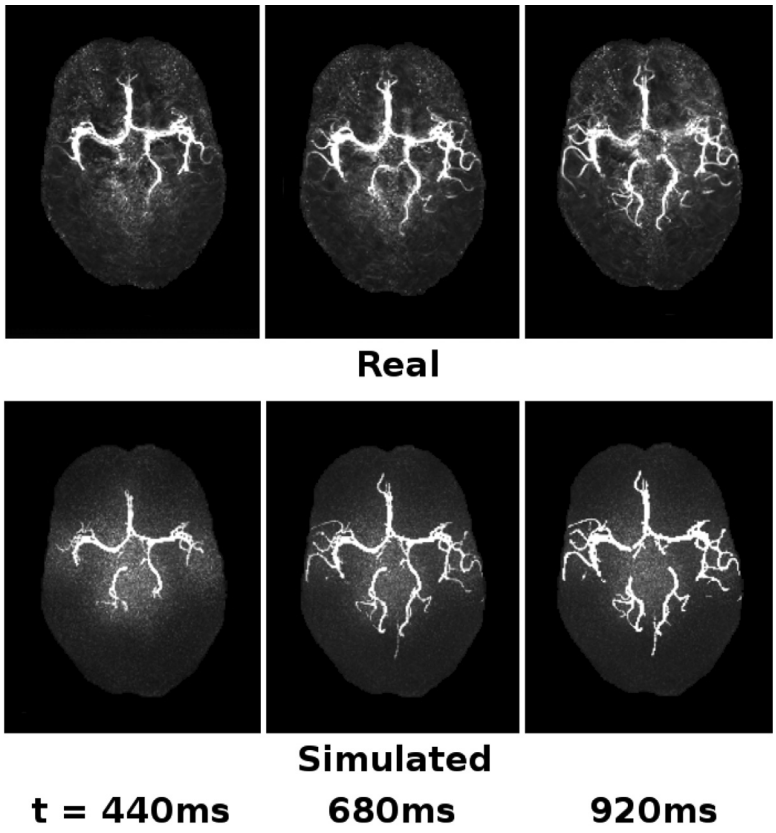

Fig. 5. Maximum intensity projections of three images of real and simulated 4D ASL MRA datasets, for t = 440, 680, and 920 ms (scenario 1).

values smaller than 1, which are common in these experiments, are assigned even smaller values when squared. In such a case, too small values might not be accurately represented due to physical limitations of the hardware being used for the experiments, and lead to erroneous parameter estimations. After identification of the optimal curve fitting parameters, the AAE between the estimated and ground-truth values for parameters $A(u)$, δ_t, s, and p is also calculated and averaged across all voxels in the binary segmentations in each scenario, for comparison purposes.

It should be noted that the AAE in this work serves two different purposes. First, it is used to optimize the fitting of a temporal curve to a set of discrete points. Second, it is used to compare true and estimated blood flow parameter values resulting from the experiments. In the following, AAE will refer only to its second function.

Table 3
Average absolute error (AAE) between the estimated and ground-truth blood flow parameters in each scenario, for vessels with a diameter larger or equal than 1 mm. The optimal values in each column are in bold.

Scenario	A(u) (*a.u.*)	δ_t (ms)	s (s^{-1})	p (ms)
1	4.74 ± 3.42	61.47 ± 51.03	2.14 ± 1.74	2.89 ± 1.91
2	5.21 ± 3.53	64.55 ± 58.66	2.23 ± 1.83	2.93 ± 2.01
3	5.64 ± 4.42	66.86 ± 58.20	2.85 ± 1.80	2.95 ± 2.09
4	5.43 ± 3.71	70.67 ± 56.41	2.76 ± 1.82	3.09 ± 2.00
5	4.52 ± 3.33	31.82 ± 19.70	1.89 ± 1.53	1.91 ± 1.22
6	5.00 ± 3.41	31.11 ± 24.99	1.99 ± 1.52	1.89 ± 1.48
7	4.99 ± 3.37	34.01 ± 24.62	1.98 ± 1.45	2.01 ± 1.16
8	5.29 ± 3.55	36.18 ± 22.77	2.11 ± 1.63	2.20 ± 1.58
9	**4.13 ± 3.17**	**21.01 ± 13.62**	**0.93 ± 0.75**	**1.05 ± 0.92**
10	4.23 ± 3.26	24.99 ± 14.80	0.93 ± 0.81	1.06 ± 0.81
11	4.45 ± 3.30	24.01 ± 14.75	0.98 ± 0.82	1.10 ± 0.81
12	4.79 ± 3.16	26.05 ± 16.66	0.97 ± 0.98	1.22 ± 0.85

4. Results

Fig. 5 shows axial maximum intensity projections of three frames from a real and a simulated 4D ASL MRA dataset. Both present the same vascular geometry, obtained from the same patient. The dynamics and dispersion of blood follows a similar pattern, but not exactly the same, as the real dataset depends on blood flow parameters of a specific subject, while the simulated datasets were generated using population average blood flow velocities, and assumed a blood flow model designed for 4D ASL MRA series (Okell et al., 2010), which may not perfectly represent reality. In terms of the noise pattern, the homomorphic approach (Aja-Fernández et al., 2015) used to generate the noise is capable of capturing the more pronounced noise signal noticeable in real datasets in the central region of the brain, around the circle of Willis, compared to the border. This pattern is a consequence of the multi-coil acquisition of the datasets, and subsequent SENSE reconstruction, which can be difficult to simulate with other approaches (Phellan et al., 2018a).

With respect to the results of the method for quantitative blood flow parameters estimation, the resulting AAE for $A(u)$, δ_t, s, and p for each scenario are presented in the following tables. Table 3 shows the AAEs in arteries with a diameter larger or equal than 1 *mm*, and Table 4 shows the AAEs in arteries with a diameter smaller than 1 *mm*.

In general, it can be noticed that all blood flow parameters: $A(u)$, δ_t, s, and p are more accurately estimated in case of large vessels, when compared to small vessels. It can also be noted that all blood flow parameters can be estimated with improved accuracy (measured by AAE) when the labeling time is set to its longest value of 3000 *ms*, which holds true for large and small vessels. Additionally, in each set of scenarios with the same labeling time: 1–4, 5–8, and 9–12, the AAE decreases when the temporal resolution r is increased, such that the lowest AAE is reached when r is set

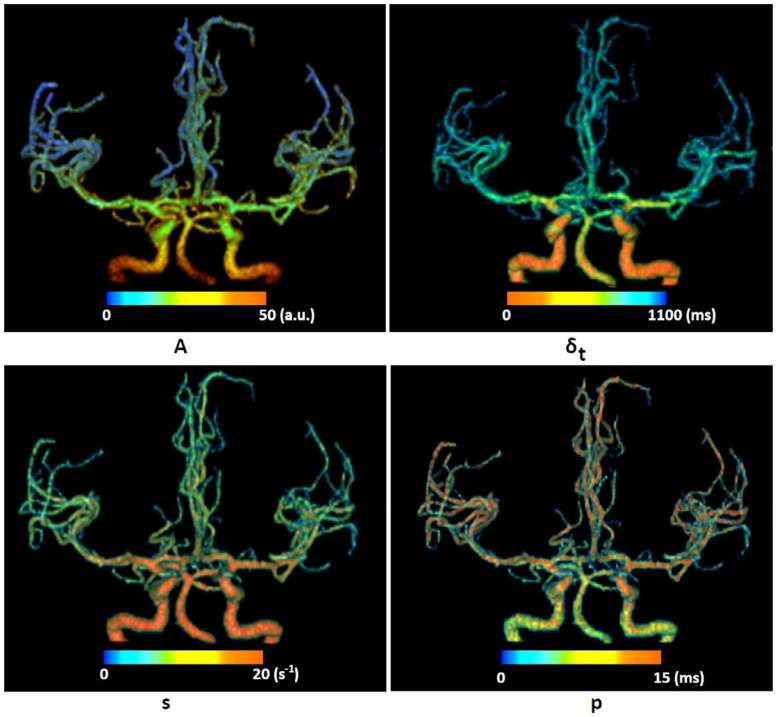

Fig. 6. 3D visualizations of the estimated blood flow parameters in scenario 9 for one volunteer.

Table 4
Average absolute error (AAE) between the estimated and ground-truth blood flow parameters in each scenario, for vessels with a diameter smaller than 1 mm. The optimal values in each column are in bold.

Scenario	A(u) (*a.u.*)	δ_t (ms)	s (s^{-1})	p (ms)
1	6.08 ± 6.36	73.84 ± 77.26	3.17 ± 2.83	3.19 ± 3.18
2	6.29 ± 6.02	75.43 ± 76.67	3.19 ± 2.49	3.47 ± 3.68
3	6.29 ± 6.07	74.58 ± 75.47	3.43 ± 2.35	3.53 ± 3.58
4	6.24 ± 6.99	82.71 ± 80.92	3.45 ± 2.44	3.68 ± 3.99
5	5.56 ± 4.25	47.19 ± 32.76	2.41 ± 1.63	2.23 ± 2.65
6	5.48 ± 4.23	47.89 ± 36.88	2.63 ± 1.74	2.31 ± 2.62
7	5.52 ± 4.27	45.24 ± 41.60	2.52 ± 1.55	2.50 ± 2.67
8	5.77 ± 4.59	54.63 ± 47.64	2.73 ± 1.86	2.52 ± 2.61
9	**4.88 ± 3.63**	**26.00 ± 24.84**	1.36 ± 0.80	**1.28 ± 1.01**
10	4.95 ± 3.65	27.05 ± 24.74	**1.24 ± 0.77**	1.29 ± 1.10
11	5.02 ± 3.78	29.37 ± 24.66	1.29 ± 0.84	1.33 ± 1.13
12	5.07 ± 3.84	30.93 ± 24.59	1.38 ± 0.79	1.46 ± 1.22

to 35 ms. This finding is also valid for both, small and large vessels. Consequently, the lowest AAE is reached when the blood is labeled for 3000 ms and the datasets are acquired with a temporal resolution of 35 ms.

Nevertheless, some exceptions to these general trends can also be observed. The parameter $A(u)$ is estimated, in larger vessels, with a lower AAE in some scenarios with a labeling time of 300 ms (1 and 2), compared to scenarios with a longer labeling time of 1000 ms (6, 7, and 8), independently of the temporal resolution. This is not the case for small vessels, where longer labeling times always lead to lower AAEs, for any parameter.

A second exception is that in some scenario sets using the same labeling time, the AAE does not always decrease when the temporal resolution is increased. This can be seen in large vessels in scenarios 4 and 7 for parameter $A(u)$; 6 and 11, for δ_t; 4, 7, and 12 for s; and 6 for p. The same result is present in small vessels in scenarios 3, 4, 6, and 7 for parameter $A(u)$; 3 and 7 for δ_t; and 7, 10, and 11 for s. These exceptions do not seem to depend on the size of the vessel considered.

The final exception is that the lowest AAE is not reached in small vessels, for parameter s, when the blood is labeled for 3000 ms and the datasets are acquired with a temporal resolution of 35 ms, but when using a temporal resolution of 55 ms.

Fig. 6 shows illustrations of estimated blood parameters from Scenario 9. Here, it becomes apparent that the parameters $A(u)$ and δ_t follow an expected behavior, with increased relative blood flow in large vessels, and early transit times in vessels closer to the neck. The parameter s also behaves as it is expected, because the large vessels closer to the labeling plane are expected to presented lower dispersion of labeled blood than peripheral vessels, and lower dispersion is associated, in this case, with higher values of s. Generally, labeled blood disperses as it travels from the labeling plane to other peripheral regions of the cerebrovascular system (Okell et al., 2010). Finally, the estimated time-to-peak p presents a more noisy pattern, but it can be seen, in general, that vessels closer to the labeling plane are assigned a lower value of p, which is also associated with lower dispersion.

As a last consideration, the required time for acquisition of the 4D ASL MRA dataset in each scenario was determined by employing the corresponding acquisition parameters on the same scanner used to acquire the real 4D ASL MRA datasets used as reference in this project. The resulting acquisition times in minutes are: 19, 10, 7, 5, 29, 16, 11, 8, 82, 57, 33, 25 min, for scenarios 1–12, in that order. In general, it can be noticed that the acquisition time increases when higher temporal resolution and longer labeling times are used.

5. Discussion

The present paper describes a methodology for the generation of virtual 4D ASL MRA phantoms that uses real vascular geometries, a mathematical model designed to describe the 4D ASL MRA signal of magnetically labeled blood flowing through the arteries of the brain, and a homomorphic approach to simulate spatially variant noise, present in images acquired with multiple coils

and SENSE reconstruction. Given the detailed control over the acquisition parameters for the phantom generation, a use example was presented, where the phantoms are employed to evaluate a method for blood flow parameters estimation in multiple image acquisition scenarios. Each scenario is created according to different settings described in the scientific literature without having to scan participants multiple times on an MRI scanner, which can be a time-consuming and expensive procedure.

The real 4D ASL MRA datasets acquired for reference purposes and the virtual phantoms present the same vascular geometry, as the latter are based on vascular segmentations obtained from high spatial resolution TOF MRA images of the same volunteers, using a validated method (Forkert et al., 2013). The blood flow dynamics are not exactly the same in corresponding real and simulated datasets, but this is an expected result, as the underlying blood flow velocities are different in both cases. In the real dataset, the blood flow parameters correspond to a particular subject, while in the simulated dataset, they are specified using population normative values (MacDonald and Frayne, 2015; Zarrinkoob et al., 2015). Additionally, in case of small vessels within the LPCA, RPCA, LMCA, and ACA regions, blood flow is distributed equally at branching points, seeking to conserve the mass of blood in the system. To the best of our knowledge, no publications have reported the blood flow distribution in these small vessels, as small vessels are highly variable in between subjects.

In terms of noise patterns, generating the virtual phantoms in 3D TOF MRA space, and then resampling the datasets to the lower resolution 4D ASL MRA space introduced partial volume effects, which are expected in a real scenario. On the other hand, assuming a probabilistic distribution for noise, such as the Rician distribution, is a common practice in literature (Gudbjartsson and Patz, 1995). In particular, this work uses a homomorphic approach (Aja-Fernández et al., 2015), which is capable of correctly simulating the more pronounced noise signal noticeable in real datasets in the central region of the brain, around the circle of Willis. This noise pattern is a consequence of the multi-coil SENSE acquisition of the datasets, and can be difficult to simulate, as noted in our previous publication (Phellan et al., 2018a).

As it can be noted, the proposed methodology for 4D ASL MRA phantom creation is flexible enough to allow replacing any method used in the separate steps of the phantom generation, if needed, shown in Fig. 1. In particular, considering that the phantoms were created and compared using data from healthy volunteers, the question of how well the 4D ASL MRA simulations would represent patients that present cardiovascular diseases still needs to be evaluated. The blood flow dynamics of patients that present disease can be represented by more complex models (Cebral et al., 2005), which could also be used in the proposed phantom generation methodology. Nevertheless, some other phenomena minimally present in healthy patients, such as motion of the subject during image acquisition, are not considered in the methodology.

The main advantage of the simulated datasets is that all acquisition and blood flow parameters can be controlled and used as a ground-truth for initial validation of medical image processing methods. Consequently, this work also shows an example where a method for blood flow parameter estimation is evaluated using the phantoms. It is observed that the relative blood volume, transit time, sharpness, and time to peak of the distribution that models the dispersion of magnetically labeled blood flowing through an artery can be more accurately estimated by the proposed method when the magnetic label is applied for a longer time. In particular, a long labeling time of 3000 *ms* allows magnetically labeled blood to fill all arteries in a healthy brain before acquiring the 4D ASL MRA series, so that the magnitude of the measured signal acquired with such a long labeling time is decreasing with time, as labeled blood flushes out of the vascular system. This approach allows all time points of the curve that describe the signal evolution of any voxel corresponding to an artery to present non-zero values, which allows a more accurate blood flow model fitting.

In contrast to this finding, a labeling time of 300 ms implies that voxels corresponding to distal arteries present zero values in the initial sample points of their signal evolution curve. The more zero values a curve presents, the more difficult it is to optimize the curve fitting problem for the blood flow model used in this work. This happens because more than one combination of the blood flow parameters to be estimated in each scenario ($A(u)$, δ_t, s, and p) may lead to a result that closely represents the reference 4D ASL MRA signal, if it contains too many zero values, and it is difficult to discriminate between them to identify the optimal combination of parameters.

For example, lets consider a peripheral artery section with a transit time δ_t of 915 ms. Assuming a labeling time τ of 300 ms, and that images are acquired from $t = 320$ ms to 920 ms, corresponding to scenario 4, with a temporal resolution of 120 ms, the resulting signal curve will only contain one non-zero value, e.g. $\{0.00, 0.00, 0.00, 0.00, 0.00, 1.88 \times 10^{-6}\}$. This curve can be modelled with Eq. (2), with considerably different blood flow parameter configurations for $[A(u), \delta_t, s, p]$, e.g. [59, 915, 5, 9] and [71, 915, 8, 8]. On the contrary, the same artery section, with a transit time δ_t of 915 *ms*, but imaged using a labeling time of 1000 *ms*, with images acquired from $t = 1015$ ms to 2095 ms, with temporal resolution of 120 ms, corresponding to scenario 8, would generate the curve {0.25, 0.17, 0.11, 0.07, 0.05, 0.03, 0.02, 0.01, 0.00, 0.00} for the parameter set [59, 915, 5, 9], and {0.21, 0.14, 0.09, 0.06, 0.04, 0.03, 0.02, 0.01, 0.00, 0.00} for the parameter set [71, 915, 8, 8]. These last two curves present more non-zero values, which allows improved hemodynamic model fitting to differentiate and select the most accurate blood flow parameter configuration.

The results of this work also suggest that the temporal resolution is a crucial parameter for accurate blood flow analysis in 4D ASL MRA datasets. More precisely, all blood flow parameters are more accurately estimated with higher temporal resolutions. Particularly, a temporal resolution of 35 ms generates the lowest AAE in the evaluated scenarios, and the error increases for the lower temporal resolutions of 50 ms, 90 ms, and 120 ms. The reason for this finding can be ascribed to the higher number of images resulting from a higher temporal resolution, which allows more accurate curve fitting results and corresponding blood flow parameter estimations.

From the previous observations, it can be concluded that longer labeling times and higher temporal resolutions lead to more accurate estimations using the evaluated blood flow parameter estimation method. This is a reasonable conclusion that would also be expected if real annotated datasets were used, showing the utility of the virtual phantoms for initial evaluation of medical image processing methods. In this paper the use example focuses on blood flow parameter estimation, within a previously segmented vascular region. However, given that the virtual 4D ASL MRA phantoms have vascular geometry and blood flow parameters ground-truth annotations, they can also be used to evaluate methods that focus on vascular segmentation, or combined segmentation and blood flow parameter estimation.

An additional aspect that needs to be considered is that in real scenarios, increasing the temporal resolution leads to a lower signal-to-noise ratio (SNR) in later time points of a 4D ASL MRA dataset. In order to compensate for this loss in SNR, more images have to be acquired and averaged, thus, prolonging the total acquisition time. Consequently, it can be observed in the results of the experiments that using higher temporal resolutions to acquire the 4D ASL MRA datasets leads to longer acquisition times. Additionally, in this project, all scenarios with the same labeling time are also assigned the same TR independently of the

temporal resolution. As an alternative that can be tested to generate the phantoms using the code available for this project (Phellan, 2019) the TR can be shortened as the temporal resolution increases. This modification will reduce the SNR of later time points as more imaging pulses are applied to the magnetically labeled blood, while potentially reducing the acquisition time of a 4D ASL MRA dataset.

Regarding the limitations of the proposed methodology, first, it assumes plug flow in the cerebrovascular system. However, the spatial resolution of 4D ASL MRA datasets is not good enough for actually displaying laminar flow properties, so that it is believed that assuming plug flow does not represent a practical limitation when analyzing real or simulated 4D ASL MRA datasets. Moreover, from a technical and theoretical perspective, simulating correct laminar flow properties would require a detailed computational fluid dynamics simulation of the whole vascular system, which is not feasible given the computational power requirements but also the need for a perfect vessel segmentation, even including microvascular structures (e.g. arterioles), which is not possible given current *in-vivo* imaging modalities.

Second, the proposed methodology assumes no mixing of blood occurs in the cerebrovascular system. Mixing of blood from different arteries practically occurs mostly within the circle of Willis in the human brain. However, the circle of Willis is only partly developed in many people. Even if it is fully developed, there might be only minimal flow in healthy conditions. In order to fully account for possible mixing, one would also have to take into account leptomeninges as well as other collateral connections within the cerebroarterial system. Then, it would be very challenging to account for all of these factors correctly because it is not feasible to obtain sufficient *in-vivo* measurements of the exact properties. However, in healthy subjects blood mixing and blood flow through other collateral connections are known to have a rather small effect compared to the blood flow from the major arteries.

6. Conclusion

In conclusion, this work presented a method to generate simulations of 4D ASL MRA annotated datasets. The annotations include ground truth data of the vascular geometry and blood flow parameters of each dataset. The annotated simulations can be used to evaluate medical image processing methods. In particular, this work presented a use example, where the phantoms were used to measure the accuracy of a blood flow parameter estimation method in various scenarios with different acquisition parameters. It was noticed that the blood flow parameters were more accurately estimated when the blood is magnetically labeled for longer times, and the datasets are acquired with a higher temporal resolution, as it would be expected if real annotated datasets were employed.

Declaration of Competing Interest

The authors declared no potential conflicts of interest with respect to the research, authorship, and/or publication of this article. Michael Helle is employed by Philips Research. Thomas W. Okell is the author of a US patent licensed to Siemens Healthcare that aims to quantify blood flow rates from angiographic data, which relies upon a kinetic model such as that used in this study.

Acknowledgments

This work was supported by Natural Sciences and Engineering Research Council of Canada (NSERC), Hotchkiss Brain Institute (HBI), and Alberta Innovates. Dr. Nils D. Forkert is funded by Canada Research Chairs. Dr. Alexandre X. Falcão thanks CNPq 302970/2014-2 and FAPESP 2014/12236-1.

References

Aja-Fernández, S., Pie, T., Vegas-Sánchez-Ferrero, G., et al., 2015. Spatially variant noise estimation in MRI: a homomorphic approach. Med. Image Anal. 20 (1), 184–197.
Aja-Fernández, S., Vegas-Sánchez-Ferrero, G., Tristán-Vega, A., 2014. Noise estimation in parallel MRI: GRAPPA and SENSE. Magn. Reson. Imaging 32 (3), 281–290.
Cebral, J.R., Castro, M.A., Burgess, J.E., Pergolizzi, R.S., Sheridan, M.J., Putman, C.M., 2005. Characterization of cerebral aneurysms for assessing risk of rupture by using patient-specific computational hemodynamics models. Am. J. Neuroradiol. 26 (10), 2550–2559.
Cocosco, C.A., Kollokian, V., Kwan, R.K.-S., Pike, G.B., Evans, A.C., 1997. Brainweb: online interface to a 3D MRI simulated brain database. In: NeuroImage. Citeseer, p. 1.
Department of informationevidence and research of the World Health Organization, 2017. WHO Methods and Data Sources for Country-Level Causes of Death 2000–2015. Report No. 2016.3, Geneva
Falcão, A.X., Stolfi, J., de Alencar Lotufo, R., 2004. The image foresting transform: theory, algorithms, and applications. IEEE Trans. Pattern Anal. Machine Intell. 26 (1), 19–29.
Forkert, N., Säring, D., Fiehler, J., Illies, T., Möller, D., Handels, H., 2009. Automatic brain segmentation in time-of-flight MRA images. Methods Inf. Med. 48 (05), 399–407.
Forkert, N.D., Fiehler, J., Ries, T., Illies, T., Möller, D., Handels, H., Säring, D., 2011. Reference-based linear curve fitting for bolus arrival time estimation in 4D MRA and MR perfusion-weighted image sequences. Magn. Reson. Med. 65 (1), 289–294.
Forkert, N.D., Schmidt-Richberg, A., Fiehler, J., Illies, T., Möller, D., Säring, D., Handels, H., Ehrhardt, J., 2013. 3D cerebrovascular segmentation combining fuzzy vessel enhancement and level-sets with anisotropic energy weights. Magn. Reson. Imaging 31 (2), 262–271.
Gudbjartsson, H., Patz, S., 1995. The rician distribution of noisy MRI data. Magn. Reson. Med. 34 (6), 910–914.
Hagen, G., 1839. Ueber die bewegung des wassers in engencylindrischen röhren. Ann. Phys. 122 (3), 423–442.
Hamarneh, G., Jassi, P., 2010. Vascusynth: simulating vascular trees for generating volumetric image data with ground-truth segmentation and tree analysis. Comput. Med. Imaging Graph. 34 (8), 605–616.
Kiepas, P., Sieradzki, J., 2015. MRI homomorphic noise estimation. Accessed: 28 December 2018. https://github.com/quepas/mri-homomorphic-noise-estimation.
Kopeinigg, D., Bammer, R., 2014. Time-resolved angiography using inflow subtraction (TRAILS). Magn. Reson. Med. 72 (3), 669–678.
Lu, H., Clingman, C., Golay, X., Van Zijl, P.C., 2004. Determining the longitudinal relaxation time (T1) of blood at 3.0 Tesla. Magn. Reson. Med. 52 (3), 679–682.
MacDonald, M.E., Frayne, R., 2015. Phase contrast MR imaging measurements of blood flow in healthy human cerebral vessel segments. Physiol. Meas. 36 (7), 1517.
Miraucourt, O., Salmon, S., Szopos, M., Thiriet, M., 2017. Blood flow in the cerebral venous system: modeling and simulation. Comput. Methods Biomech. Biomed. Eng. 20 (5), 471–482.
Okell, T.W., Chappell, M.A., Schulz, U.G., Jezzard, P., 2010. A kinetic model for vessel-encoded dynamic angiography with arterial spin labeling. Magn. Reson. Med. 64 (3), 698–706.
Phellan, R., 2019. Four-dimensional arterial spin labeling MR angiography virtual phantoms. Accessed: 22 May 2019. https://github.com/rphellan/4DASLMRAVirtualPhantoms.
Phellan, R., Forkert, N.D., 2017. Comparison of vessel enhancement algorithms applied to time-of-flight MRA images for cerebrovascular segmentation. Med. Phys. 44 (11), 5901–5915.
Phellan, R., Linder, T., Helle, M., Spina, T.V., Falcão, A., Forkert, N.D., 2018. Four-dimensional asl mr angiography phantoms with noise learned by neural styling. In: Intravascular Imaging and Computer Assisted Stenting and Large-Scale Annotation of Biomedical Data and Expert Label Synthesis. Springer, pp. 131–139.
Phellan, R., Lindner, T., Helle, M., Falcão, A.X., Forkert, N.D., 2018. Automatic temporal segmentation of vessels of the brain using 4D ASL MRA images. IEEE Trans. Biomed. Eng. 65 (7), 1486–1494.
Poiseuille, J.L., 1844. Recherches expérimentales sur le mouvement des liquides dans les tubes de très-petits diamètres. Imprimerie Royale.
Robson, P.M., Dai, W., Shankaranarayanan, A., Rofsky, N.M., Alsop, D.C., 2010. Time-resolved vessel-selective digital subtraction MR angiography of the cerebral vasculature with arterial spin labeling. Radiology 257 (2), 507–515.
Ruppert, G.C., Chiachia, G., Bergo, F.P., Favretto, F.O., Yasuda, C.L., Rocha, A., Falcão, A.X., 2017. Medical image registration based on watershed transform from greyscale marker and multi-scale parameter search. Comput. Methods Biomech. Biomed. Eng. 5 (2), 138–156.
Zarrinkoob, L., Ambarki, K., Wåhlin, A., Birgander, R., Eklund, A., Malm, J., 2015. Blood flow distribution in cerebral arteries. J. Cereb. Blood Flow Metab. 35 (4), 648–654.